ACS APPLIED POLYMER MATERIALS

pubs.acs.org/acsapm

Article

Nanostructured Effect on Antifouling Conducting Polymers through Interfacial Adhesive Interaction and Protein Adsorption

Chia-Hsin Lin, Chang-Yun Wang, Jie-Ren Li,* and Shyh-Chyang Luo*

Cite This: *ACS Appl. Polym. Mater.* 2023, 5, 10105−10115

Read Online

ABSTRACT: Antifouling properties are indispensable for ensuring the efficiency of biomedical applications in biotechnology. Bioinspired antifouling surfaces have undergone significant development. The adhesive interactions of nanopatterns supply localized force-related data. In this study, a precisely defined conducting polymer (CP), poly(3,4-ethylenedioxythiophene) (PEDOT), was enriched with antifouling phosphorylcholine moieties (PEDOT-PC) for comparison with hydroxyl-functionalized PEDOT (PEDOT-OH) to investigate their effects. Well-defined nanopatterned PEDOT films can be precisely created by controlling the electropolymerization process on a polystyrene (PS) monolayer template using a colloidal lithography approach. Electropolymerized PEDOT coatings have emerged as a surface modification strategy for bioelectrodes due to their facile functionalization and fabrication. The patterns are versatile, depending on the sizes of PS beads and electropolymerization conditions. Atomic force microscopy (AFM) allows for the examination of the adhesion effects of periodic nanostructures in aqueous solutions. Real-time and quantitative assessment of adhesion between the AFM tip and the sample was conducted through force−volume mapping. Furthermore, the study involved the examination of protein adsorption behaviors at these interfaces using a quartz crystal microbalance with dissipation (QCM-D), including bovine serum albumin (BSA), cytochrome *c* (cyt *c*), lysozyme (LYZ), and C-reactive protein (CRP). AFM probing near the interface revealed that surface morphology induced higher adhesion forces than pristine polymer films, whereas the PEDOT-PC coating exhibited minimal interaction during tip scanning. Additionally, protein adsorption tests indicated that the nanostructures compromised the antifouling properties of PEDOT-PC films, aligning with water contact angle measurements. The periodic structure enhances the energy barrier, disrupting the preservation of a continuous water layer captured by the PC moieties. Our research offers a straightforward approach to creating a nano CP template suitable for various systems. Moreover, it provides a deeper understanding of the physical investigation and the implications of biomolecule responses of the nanostructure effects using AFM and QCM-D.

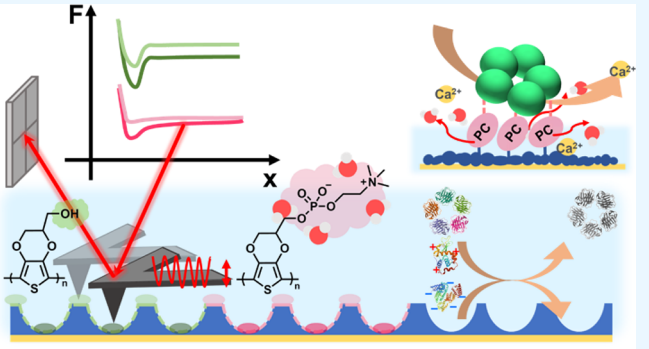

KEYWORDS: *nanostructure, AFM, conducting polymer, PEDOT, adhesive force, biointerface*

1. INTRODUCTION

Nanotechnology, specifically when applied within the nanometer scale, offers valuable insights into the fundamental aspects of chemistry and biology. In biotechnology, environmental alterations can significantly influence biomolecular interaction dynamics including protein adsorption and cellular function. Above all, the interface environment facilitates communication between the solid substrate and the surrounding liquid environment. The natural creature has inspired many biomimetic surfaces. One of the well-known phenomena is the Lotus effect.[1,2] The periodic patterns give rise to their exceptional water repellency and self-cleaning ability. This concept has been applied to develop superhydrophobic surfaces in various applications. Well-defined biointerfaces have attracted great interest and have been researched for decades.[3−6] There are numerous methods to create a textured surface. In this study, we used colloidal lithography to prepare the substrate. Colloidal lithography is a nanofabrication technique that uses self-assembled monolayers of colloidal particles such as polystyrene (PS) beads to create patterns on a substrate. PS beads are dispersed in a solvent with a uniform size. The solvent is then allowed to evaporate, leaving behind a layer of beads on the substrate. As a result, PS beads can be easily transferred to any desired substrate. As the solvent evaporates, capillary forces come into play, causing the beads

Received: August 23, 2023
Revised: October 23, 2023
Accepted: October 26, 2023
Published: November 9, 2023

https://doi.org/10.1021/acsapm.3c01964
ACS Appl. Polym. Mater. 2023, 5, 10105−10115

to self-assemble into a regular array or pattern on the substrate.[7−12] Colloidal lithography using PS beads offers several advantages, including its simplicity, cost-effectiveness, and the ability to achieve nanoscale patterning.

Surface treatment is vital in bioapplications, especially when undesired biomolecular fouling is prevented on pristine material surfaces. The adhesion of undesirable substances can significantly compromise the functionality of the devices. Regarding implants, adhesion in such cases can cause aggregation, which may lead to clotting and potentially result in thrombosis.[13] Zwitterionic molecules, intrinsically carrying both positive and negative charges, have an excellent antifouling ability to resist the binding of undesirable biomolecules.[13−15] Phosphorylcholine (PC) is inspired by the hydrophilic polar headgroup of the phospholipid bilayer on the cell membrane. 2-Methacryloyloxyethyl phosphorylcholine (MPC) is a well-known vinyl molecule with a zwitterionic PC moiety, and the methacrylate can be designed for various architectures via polymerization techniques.[16] In recent studies, PC has shown its stability, and there are versatile methods to incorporate PC with soft materials.[17,18] A zwitterionic functional group PC can also be synthesized and incorporated into 3,4-ethylene dioxythiophene.[19] Poly(3,4-ethylenedioxythiophene) (PEDOT) is a conducting polymer (CP) that has gained significant attention in various fields. This CP possesses several advantages, such as low impedance, in vitro and in vivo biocompatibility, high electrical conductivity, and tunable properties. It is worth mentioning that PEDOT can incorporate versatile, functional groups, allowing bioconjugation.[20,21] A hydrophilic monomer can be readily polymerized, leading to the formation of phosphorylcholine functionalized poly(3,4-ethylenedioxythiophene) (poly(EDOT-PC)). This coated surface creates a high electrical and ionic conductivity interface with high resistance toward nonspecific binding.[22,23]

To investigate the surface properties of biomaterials, atomic force microscopy (AFM) is a powerful and versatile technique for high-resolution imaging and surface characterization. In previous studies, the AFM technique shows potential to evaluate the water structure of the solid−liquid interface, including 3D mapping.[24,25] In particular, the Peak Force Quantitative Nanomechanical (QNM) mode within AFM enables the assessment of adhesive forces between the probe tip and the sample surface. Utilizing the QNM mode, the AFM probe tip intermittently contacts the sample surface, employing a precisely controlled force.[26] Valuable information about adhesive interactions can be obtained by monitoring the deflection of the cantilever, which is directly correlated to the adhesive forces experienced between the tip and the surface. Additionally, it offers the ability to generate adhesive force maps that reveal variations in strength and distribution.[27] This information is crucial for understanding the thorough properties of surfaces, enabling advancements in various fields such as materials science, biomaterials, and nanotechnology.[28]

On the other hand, the study of protein binding and its behavior has extensively utilized a quartz crystal microbalance with dissipation (QCM-D) module system. QCM-D is a susceptible technique for measuring real-time protein adsorption on solid surfaces. The additional dissipation module provides valuable information about the mass and viscoelastic properties of the adsorbed protein layer. In general, the viscoelastic properties are quantified by dissipation shift (ΔD) curves, and the binding amount of the analytes to interfaces is the frequency shift (ΔF). QCM-D enables the investigation of various aspects of protein adsorption, including adsorption kinetics, protein conformational changes, layer thickness, and viscoelastic properties.[29−31] QCM-D is widely used in multiple fields, including biophysics, biomaterials, and biochemistry, to gain fundamental insights into protein−surface interactions, as well as to guide the design and optimization of biomaterials, biosensors, and other biomedical applications.[32−34]

On the basis of prior research, the antifouling coatings were used or developed for a relatively large scale of over a micrometer or a roughening interface and gave effective antifouling properties.[35] The nanopatterns usually enhance the hydrophilicity of a hydrophilic surface (<90°) or hydrophobicity of a hydrophobic surface (>90°). Nevertheless, comprehensive research on the impact of nanostructures and their connection to the antifouling properties within antifouling coatings is limited.[36] The promising antifouling materials can form a hydration layer due to the local positive and negative ion pairs on the molecular design of zwitterions, which are more effective than hydrogen bonding. However, several factors regulate the wetting ability on the interface, such as grafting density and surface roughness factor.[37,38] In this study, a surface with a regular nanopattern might induce a hydrophobic interaction on a hydrophilic CP coating by investigating the adhesive interaction. After the CP interface with periodic patterns was created, QNM mode in a liquid environment and QCM-D measurement were used to characterize the patterned surface. This research offered direct information using AFM probing through the solid−water interface and a comprehensive understanding of the intricate relationship between nanostructures and protein−surface interactions. Furthermore, the investigation delves into the synergistic effect of the combination of hydrophobic nanostructures and hydrophilic surface decoration.

2. EXPERIMENTAL SECTION

2.1. Chemicals and Reagents. Two sizes of PS microbeads (diameters of 200 and 50 nm sizes with 2.5% solid (w/v) aqueous suspension with minimal surfactant) were purchased from Polysciences, Inc., without further purification. The recombinant CRPs were purchased from Prospec-Tany (Rehovot, Israel). Hydroxymethyl EDOT (EDOT-OH), BSA, lysozyme from chicken egg white (LYZ), cytochrome *c* from the equine heart (cyt *c*), and calcium chloride were purchased from Sigma-Aldrich (USA). Dioctyl sodium sulfosuccinate, dodecyl sulfate, sodium salt, HEPES, and sodium chloride were purchased from Acros. Tetrabutylammonium perchlorate (TBAP) was purchased from Tokyo Chemical Industry Co., Ltd. Lithium perchlorate and acetonitrile (ACN) were obtained from Alfa Aesar. EDOT-PC was from Dr. Hsiao-hua Yu, Academia Sinica, and the synthesizing process followed previously published procedures.[19] All the referred chemicals were used without further purification.

2.2. Nanostructured CP Film Preparation. *2.2.1. PS Nanosphere Self-assembly on the Air−Water Interface.* We applied the self-assembly method at the air−water interface to create a periodic pattern. The procedures of the colloidal lithography technique follow previous studies.[39,40] The PS nanospheres self-assembled on a QCM-D Au sensor (QSX 301). Polystyrene (PS) nanospheres were allowed to self-assemble on a QCM-D Au sensor (model QSX 301). The aqueous suspension of PS nanospheres was diluted with alcohol in a ratio of 3:2 (volume to volume) for 200 nm-sized spheres and 5:1 for 50 nm-sized spheres to minimize the overlapping of PS nanospheres. The surface was meticulously cleaned before the diluted PS nanosphere solution was dropped on the glass slide. It was rinsed with acetone and water and then subjected to a 30 s treatment with oxygen plasma to ensure cleanliness and hydrophilicity.

https://doi.org/10.1021/acsapm.3c01964
ACS Appl. Polym. Mater. 2023, 5, 10105−10115

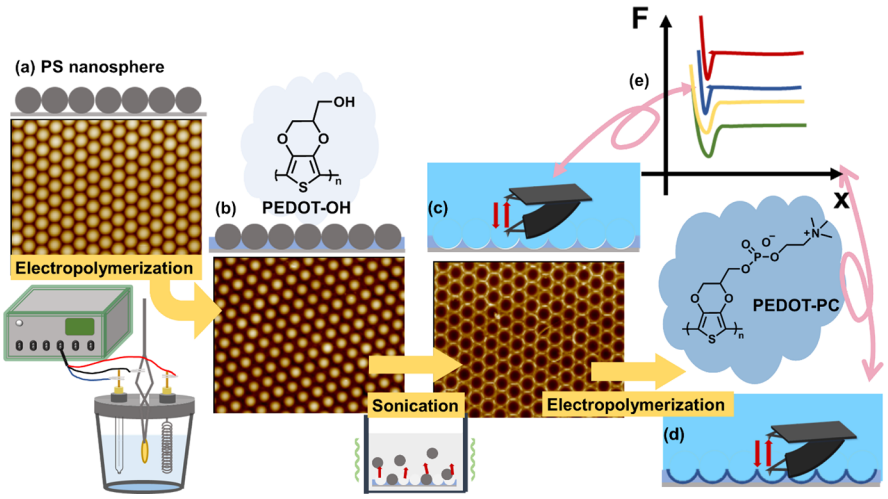

Figure 1. Flowchart of the sample preparation and characterization. (a) PS nanospheres are self-assembled at the air−liquid interface into hexagonal arrays and then transferred to a QCM chip. (b) Colloidal lithography is carried out on the PS nanosphere-masked QCM chip via electropolymerized PEDOT-OH. The CP films start to polymerize from the exposed gold, which is not covered by PS nanospheres, and then the film grows between the interspace of the PS nanosphere monolayer. Electropolymerization conditions can readily control the height of the bowl shape. (c) The PS nanosphere mask is removed by sonication in toluene. Solvent washing revealed the CP pattern that remains on the QCM substrate. The template of bowl-shaped PEDOT-OH is used for further AFM characterization (e) and protein binding test. (d) Despite PEDOT-OH, hydrophilic PEDOT-PC was further deposited for a thin layer on PEDOT-OH. (d) The PC-decorated substrate was characterized in the same way as PEDOT-OH.

A dish filled with deionized water was prepared, and the pretreated glass slide was carefully positioned in the dish at a 30° angle, with half of it exposed to the air. The PS nanosphere solution (20 μL) was gently and continuously pipetted onto the side of the glass slide facing the air. A monolayer was promptly formed as the PS microbeads came into contact with the air−water interface. The PS nanosphere monolayer became visible and expanded as the solution was continuously injected. The monolayer was left to stand for 30 min to stabilize, and then the film was scooped up from the air−water interface with a QCM Au chip. The chip was then heated to 80 °C for 1 h to accelerate the water evaporation and PS packing. This method is useful for depositing nanospheres of any size on a desired substrate.

2.2.2. Electropolymerization of CP. Two different EDOT-OH solutions were prepared, each with 50 and 200 nm size templates. The solutions comprised 10 or 50 mM EDOT-OH, 50 mM SDS, and 100 mM LiClO4 in deionized water. The electropolymerization process was carried out using an Autolab PGSTAT128N instrument from Metrohm, The Netherlands, employing a three-electrode system. For the aqueous phase, the reference electrode consisted of Ag/AgCl with saturated KCl, and a Pt wire served as the counter electrode. In the aqueous phase, the reference electrode consisted of Ag/AgCl with saturated KCl and a Pt wire as the counter electrode. The nonaqueous EDOT-PC solution was prepared by dissolving 10 mM EDOT-PC, 50 mM DSS, and 100 mM $LiClO_4$ in ACN. An Ag/Ag^+ electrode with 100 mM TBAP in ACN was used as the reference electrode in the nonaqueous solution. To create a half-covered CP structure on the 200 nm PS nanosphere monolayer, PEDOT-OH was deposited by applying a cyclic potential for one cycle, ranging from −0.4 to 0.9 V (vs Ag/AgCl) at a scan rate of 50 mV s^{-1} under room temperature in 50 mM EDOT-OH solution. The 50 nm PS-masked nanopattern was deposited with one cycle from −0.4 to 0.9 V (vs Ag/AgCl) at a faster scan rate of 80 mV s^{-1} in 10 mM EDOT-OH solution. The poly(EDOT-PC) thin layer was further deposited on the poly-(EDOT-OH) platform with one cycle from −0.4 to 1.0 V (vs Ag/AgCl) at a scan rate of 100 mV s^{-1}. The experimental setups and steps are listed in Figure 1. Fourier-transform infrared spectroscopy (FTIR) was used to characterize the chemical properties of CP films (Figure S1). In the FTIR spectra, we can observe an additional C−O stretching at 1041 cm^{-1} for PEDOT-OH, which is not visible from PEDOT. The blue curve further points out several peaks of the PC functional groups. The peaks at 970 and 1244 cm^{-1} are assignments of the positively charged choline group. The peaks at 1066 and 1093 cm^{-1} are vibrations of $C-O-PO_2^-$ and symmetric PO_2^- stretching from the negatively charged phosphate group. X-ray photoelectron spectroscopy (XPS) further characterized the elemental composition of CP thin films (Figure S2). Although the oxygens of C−O−C and C−O−H have similar binding energies due to similar electronegativities, the O 1s energy spectrum of PEDOT-OH shows a higher intensity and a slight peak shift compared with PEDOT. The cyclic voltammograms (CVs) reveal electrical properties, such as the double-layer capacitance of PEDOT-OH and PEDOT-PC films (Figure S3). The CV curves were recorded under scan rates of 25, 50, 100, 200, and 300 mV s^{-1} in an aqueous environment with 100 mM $LiClO_4$. PEDOT-OH films act as the CP template, presenting a thicker electrical double layer corresponding to the film thickness.

2.3. Characterization. The AFM measurements were conducted using a BioScope Resolve BioAFM instrument (Bruker, USA). The surface morphology was measured with tapping mode in the air using a SCANASYST-AIR silicon tip (spring constant: approximately 0.4 N m^{-1}, frequency: 70 kHz, normalized tip radius: 2 nm). Adhesion force and force volume were determined in PeakForce quantitative nanomechanical mapping (PFQNM) mode in liquid by using a DNP silicon tip with cantilever C (spring constant: approximately 0.35 N m^{-1}, frequency: 56 kHz, normalized tip radius: 20 nm). Each tip was cleaned with oxygen plasma for 30 s before doing the force−volume mode. The applied force throughout the measurement process was fixed at about 2 nN, and force−distance curves were collected with 24 × 24 pixels. The data were further analyzed using AFM NanoScope Analysis software version 1.8 (Bruker, USA). At room temperature, static contact angles were measured by using a contact angle goniometer (Sindatek, Taiwan). Three measurements were performed using 1.0 μL of deionized water droplets. The QCM-D (Biolin Scientific, Västra Frölunda, Sweden) setup consists of a quartz crystal sensor, typically a thin quartz disk with metallic electrodes on both sides. The crystal is excited at its resonance frequency, which is in the megahertz range. All the polymer films were coated on the surface of a QSX 301 QCM chip by electropolymerization and placed into the Q-sense four-channel module. All measurements were performed at room temperature and were repeated three times. The flow rate was maintained at 25 μL min^{-1} using an Ismatec ISM935C pump. Changes in frequency of the third overtone (n = 3, i.e., 15 MHz) were used for the data readout. The

https://doi.org/10.1021/acsapm.3c01964
ACS Appl. Polym. Mater. 2023, 5, 10105−10115

frequency value depends on adhered mass, which the theoretical QCM models can calculate. A relationship from a decrease in frequency means an increase in mass; on the other hand, a drop in frequency indicates that an increase in mass can occur. In this research, C-reactive protein (CRP) was specifically selected as the binding protein for PEDOT-PC. At the same time, bovine serum albumin (BSA), lysozyme (LYZ), and cytochrome *c* (cyt *c*) were categorized as nonspecific binding proteins. These nonspecific proteins were dissolved in a phosphate-buffered saline (PBS) solution at a concentration of 1 mg mL^{-1}. The CRP concentration was 4 μg mL^{-1} and dissolved in a HEPES buffer containing 1 mM $CaCl_2$. Adding an adequate amount of calcium ions was crucial for enabling CRP-PC recognition. As protein molecules adhered to the sensor surface, the additional mass induced a shift in the resonance frequency, which could be quantified and associated with the quantity of adsorbed protein. Furthermore, the energy dissipation during the oscillation provided insight into the energy loss within the protein layer.

3. RESULTS AND DISCUSSIONS

3.1. Surface Properties of 200 and 50 nm PS Nanosphere-Masked PEDOT-OH/PEDOT-PC Films. Colloidal lithography offers an uncomplicated approach to creating two sizes of PS nanosphere monolayers, each partially covered with PEDOT-OH, with remarkable precision via direct electropolymerization. To achieve a well-defined nano PEDOT pattern, we carefully optimized the experimental conditions to achieve the desired depth. Parameters such as the monomer concentration, scan rate, and upper potential are adjustable within the cyclic potential mode. The cyclic voltammetry (CV) diagram illustrated the electrodepositing process of the nanostructure at different depths (Figure S4). The upper potential applied for oxidizing the EDOT-OH monomer for these two templates was set identically. Polymerization of PEDOT-OH started at approximately +0.6 to +0.7 V within the interstitial spaces between the substrate and the PS beads. The 200 nm masked templates were formed using a slower scan rate and a five-times increase in the monomer concentration. The surface morphologies of two patterns and the control experiment of PEDOT-OH thin films were characterized by tapping mode (Figure 2a–c). The 200 nm PS nanosphere-masked PEDOT-OH presented an apparent concave-upward pattern, and the height was controlled at half or slightly lower than one PS nanosphere. The cross sections are shown in Figure S5. The pristine PEDOT-OH had a similar grain size and was presented on a similar scale as 50 nm PS nanospheres. The weight of small sizes such as 50 nm PS nanospheres was much lighter than 200 nm, which made 50 nm PS nanospheres easy to overlap at the air–water interface. This caused the 50 nm PS nanosphere-masked PEDOT-OH films to be hard to fabricate perfectly. However, compared with the cross-section images (Figure S5a,c), 50 nm PS nanosphere-masked PEDOT-OH films still presented a cavity pattern periodically, whereas pristine PEDOT-OH formed irregularly globular grains on the surface. Consequently, the WCA is determined primarily through chemical properties and surface morphology. For the PEDOT-OH film, the WCA is 61.2 ± 3.5°. After a nanostructure was created with a depth of around 100 nm, the WCA rises to 88.3 ± 6.6° and slightly decreases at the smaller nanoscale of 50 PS-masked PEDOT-OH (82.6 ± 6.4°).

For ideal flat and smooth solid surfaces, the WCA was determined by the Young–Dupre equation: $\gamma_{sv} - \gamma_{sl} = \gamma \cos \theta^{Y}$. The Young's angle ($\theta^{Y}$) was affected by only interfacial free

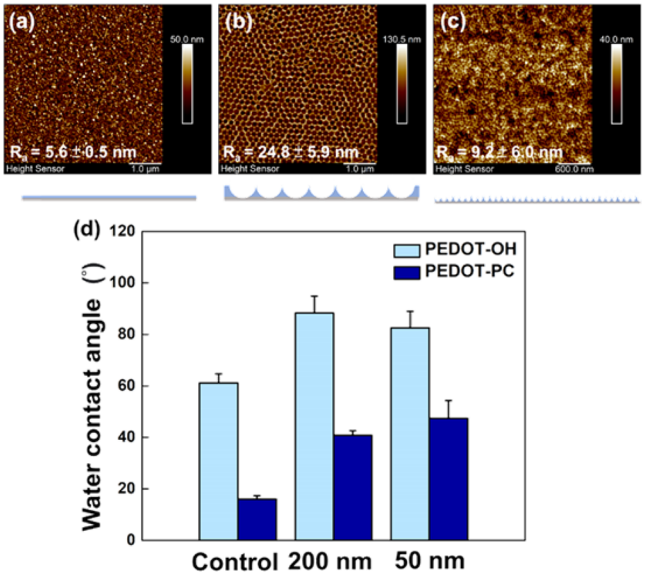

Figure 2. AFM topography images of (a) smooth PEDOT-OH film forming with one CV scan (potential: −0.4 to +1.1 V vs Ag/AgCl) compared to nanopatterned PEDOT-OH with (b) 200 nm PS nanospheres and (c) 50 nm PS nanospheres as masks. (d) The WCA results from three different substrates with PEDOT-OH (light blue) and PEDOT-PC covered (royal).

energy per unit area for the solid–vapor (γ_{sv}), solid–liquid (γ_{sl}), and liquid–vapor (γ) interface.[41] However, in another two classic wetting theories, the Wenzel and Cassie–Baxter model, the surface wettability for water was determined by an air–water interface, including surface roughness. Wenzel's theory considered a factor of surface roughness, *r* (ratio between the solid–liquid interfacial area and the projected area), and assumed that the liquid drop fills the space between the protrusions on the surface. The Wenzel equation followed the equation extended from the Young–Dupre equation: $\cos \theta_W = r\cos \theta^Y$. With increasing surface roughness, *r*, the WCAs were assumed to decrease. In contrast, the Cassie and Baxter model assumed that the space was occupied by air trapped inside the protrusions. The prediction of the Cassie–Baxter model was given by $\cos \theta_{CB} = r_f f \cos \theta + f - 1$, where r_f was the ratio of the actual surface in contact with the liquid to the projected area of the wetted region and *f* was the fraction of the liquid–solid interface in the entire composite.[41−44] In this study, 200 nm nanosphere-masked and 50 nm nanosphere-masked PEDOT-OH both behaved in larger interfacial areas according to the average roughness (R_a), whereas the WCA increased, which was incorrect to explain with the Wenzel model. As a result, the bowl shape of CP formed by the PS nanospheres corresponded more to the trend of the Cassie–Baxter model. After the PEDOT-PC covered the PEDOT-OH pattern, both surfaces became much more hydrophilic. The WCA results demonstrated the competitive relation between the chemically hydrophilic interface and nanostructure effect on water wetting ability to a platform. The nanostructure effect indicated that the numerous pits interrupted the wetting ability of the PC on the patterned interface, which caused increases in the WCA results. In summary, water wetting was a balancing process between the gas, liquid, and solid phase. The remaining spaces not thoroughly wetting on the concave-upward nanopattern may contribute to its hydrophobicity. After further deposition of a layer of PEDOT-PC, the WCA

https://doi.org/10.1021/acsapm.3c01964
ACS Appl. Polym. Mater. 2023, 5, 10105−10115

dramatically dropped. The WCAs of the nanopatterned PEDOT-PC were slightly higher than the pristine thin film, which resulted from the higher density of air-trapping sides.

3.2. PFQNM Mapping on the Bowl Shape Surface in Liquids. *3.2.1. The 200 nm PS Nanospheres-Masked Platform.* Characterization with the Peak Force tapping mode reveals the surface morphology of concave-upward PEDOT-OH/PEDOT-PC films and evaluates the adhesive force for both surfaces simultaneously. In this study, we conduct the experiment in a liquid environment. This strategy investigates the tip−sample interaction for nanostructured interfaces with a high precision and sensitivity. AFM topography and corresponding adhesion images of similar areas of concave-upward PEDOT-OH/PEDOT-PC patterns are compared side-by-side, as shown in Figure 3. Arrays of

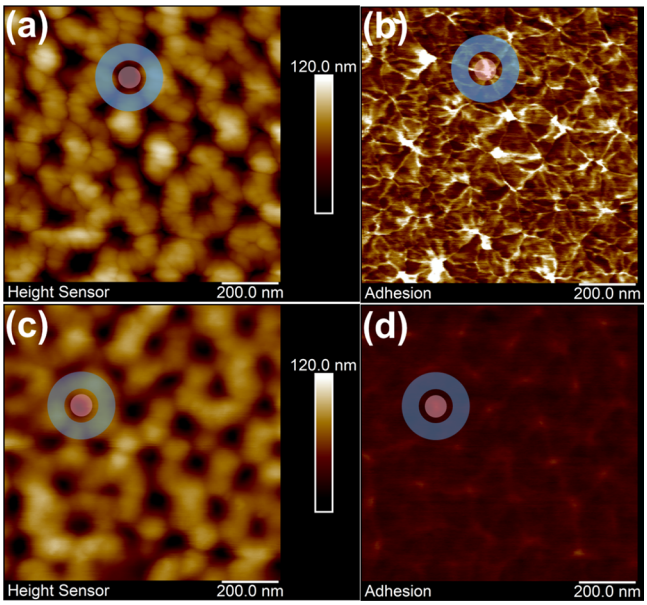

Figure 3. Peak Force mode mapping of the (a) topography and (b) adhesion of 200 nm PS nanosphere-masked PEDOT-OH nanopattern compared with the topography (c) and adhesion of the PEDOT-PC nanopattern (d). The area marked with blue indicates the top of the pattern with a lower adhesion force. The pink dots are the cavity regions, which present a higher adhesion force.

PEDOT-OH/PEDOT-PC patterns with honeycomb morphologies are observed in Figure 3a,c. Small protruding domains of PEDOT-OH/PEDOT-PC polymers that assemble to form a ring-shaped geometry by the PS particles become evident throughout areas of the surface. The pores of the rings pinpoint the locations where the individual PS particles were removed. The center-to-center spacing of the PEDOT-OH/PEDOT-PC rings conforms to the periodicity of the PS masks. Referencing the central uncovered areas of rings as a baseline, the pattern heights of the PEDOT-OH/PEDOT-PC patterns are fairly even throughout the surface, exhibiting a uniform coverage of well-defined polymeric nanopatterns. The long-range order and hexagonal arrangement of concave-upward PEDOT-OH/PEDOT-PC films are apparent, although a few defects produced by missing PS particles are noticeable.

The changes in surface chemistry between the PEDOT-OH and the PEDOT-PC rings are viewed in the adhesion images of Figure 3b,d. Adhesion images result from differences in adhesive force between the tip and the surface functional groups of polymers, providing a sensitive map of the changes in surface functionality. The bright contrast of adhesion images shown in Figure 3 represents the cavity regions of PEDOT-OH/PEDOT-PC rings highlighted in pink dots, which indicate a higher adhesion force inside those ring-shaped structures. Adhesion images can also reflect changes resulting from surface topography, such as edge effects. As the tip moves up or down across the PEDOT-OH/PEDOT-PC ring patterns, the outlines of the nanostructured structures predominate for the circular geometry, with a slightly bright contrast at the pattern edges. The edge effects are evident for the adhesion image because of changes in tip−surface interactions when the tip is scanned over the patterns, providing a precise outline of the ring geometries. The adhesion image in Figure 3b, highlighted in blue, reveals distinguishably brighter contrast at the polymeric region of the PEDOT-OH concave-upward film compared to the ambiguous, dark contrast exhibited for the PEDOT-PC nanopattern marked in the blue circle of Figure 3d. The contrast in adhesion image can be attributed to the different adhesive forces on PEDOT-OH/PEDOT-PC nanopatterns, indicating that the surface of the PEDOT-OH concave-upward film is more adhesive than the PEDOT-PC one. Even though morphological analysis with topography images exhibits a remarkably uniform pattern height and the adhesion image serves as the semiquantitative analysis to obtain a chemical contrast on surfaces, a precise and sensitive mapping of the surface functionality is necessary to distinguish and decipher the differences in adhesive properties for both polymeric surfaces.

Force−volume mapping is an AFM characterization mode that combines precise force measurement with topographic imaging.[28,45,46] The force−volume data merge nearly simultaneous topographic measurement with force information into a single data set, enabling the correlation of force with surface features. Representative force−volume mapping for PEDOT-OH/PEDOT-PC patterns in Figure 4 provides a more precise manner to identify the differences in adhesive properties for both polymeric surfaces. During the force−volume mapping process, a series of force measurements are obtained point-by-point in a grid pattern. Each force measurement can be compared directly with the corresponding topography image to generate a 3D volume map, as shown in Figure 4a,c. Force−curve profiles obtained from a $1 \times 1\ \mu m^2$ scan area (24×24 pixels) of PEDOT-OH/PEDOT-PC patterns are used to evaluate the differences in adhesive properties for both surfaces. The retraction curves from force−volume maps enable us to calculate the adhesion force between an AFM tip and each polymeric surface, as plotted in Figure 4b,d for PEDOT-OH and PEDOT-PC patterns, respectively. Adhesion is the force required to pull the tip away from the surface. The adhesive forces measured from PEDOT-OH patterns range from 0.7 to 2.0 nN for each pull-off event during retraction cycles of force curves. In contrast, weak adhesive forces are barely detectable for PEDOT-PC patterns. The force curves in Figure 4 indicate a more significant adhesion force from hydroxyl (OH) groups of PEDOT-OH versus almost no adhesion force from PC groups of PEDOT-PC.

On the basis of the evidence of structural analysis and force−volume mapping, a rational model to illustrate the contact between the AFM tip and the air−water interface is shown in Figure 4e. Conventionally, the WCA is the angle measured through a water drop on the surface where an air−liquid interface meets a solid. The WCA measurement presents

https://doi.org/10.1021/acsapm.3c01964
ACS Appl. Polym. Mater. 2023, 5, 10105−10115

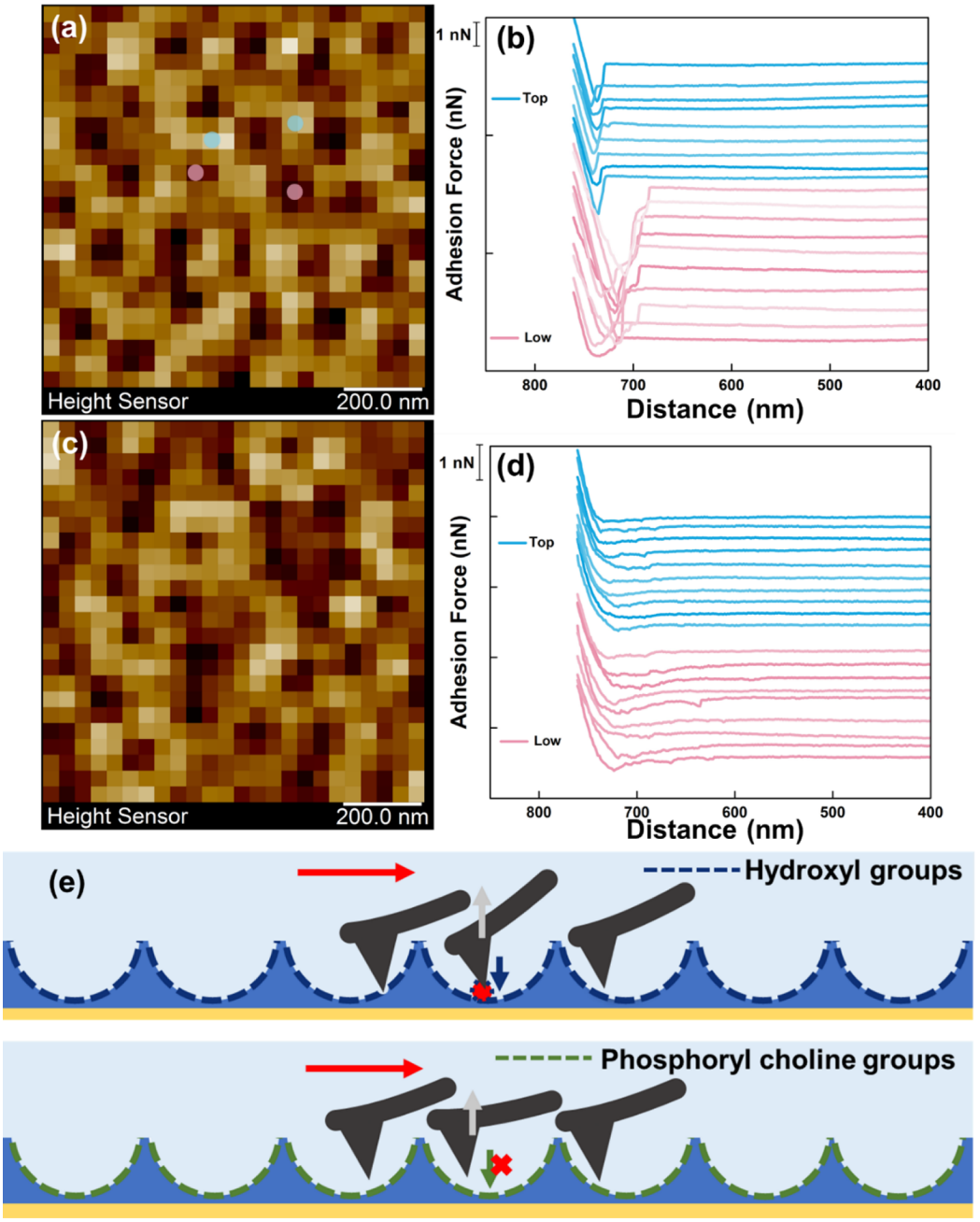

Figure 4. Force−volume mode and retraction force−distance curves on a 200 nm PS nanosphere template using AFM. (a, b) Adhesion mapping on the PEDOT-OH film. (c, d) Adhesion mapping on further depositing PEDOT-PC film. A force of 2 nN was applied throughout the measurement process with PFQNM mode in liquid. The resolution was 24 × 24 pixels in 1 μm × 1 μm. The blue force curves were chosen from the bright pixels, and the pink curves were selected on the dark region of the topography. Ten force−distance curves were shown as panels b and d. (e) Schematic of the illustration for the contact−water interface.

the balance of the gas, liquid, and solid phases. For force−volume mapping, the sample is completely immersed in the liquid followed by the force−curve measurement on the sample surface with an AFM tip at the nanometer level. Because the liquid thoroughly infiltrates the surface, no air bubbles should exist inside the PEDOT-OH/PEDOT-PC concave-upward patterns. As the AFM tip comes into contact with a nanobubble before touching the substrate, the tip−bubble interaction exhibits a linear slope in the deflection-height sensor curve.[47−50] However, no linear slope appears in the deflection-height sensor curve, as shown in Figure 4b,d. The AFM tip senses no repulsive force from a nanobubble as the tip scans the PEDOT-OH/PEDOT-PC concave-upward patterns in liquid. Force−curve profiles enable the detection of a more significant adhesion force from PEDOT-OH due to hydrogen bonding between the OH groups and the AFM tip. PC groups of PEDOT-PC prevent adhesion forces to the AFM tip. The model in Figure 4e illustrates that force-volume mapping in liquids enables the probe of the AFM tip's contact with the water−air interface and directly reveals the differences in surface adhesion due to surface functional groups.

3.2.2. The 50 nm PS Nanosphere-Masked Platform. In Figure S6, we also conducted AFM mapping in a liquid environment on a 50 nm PS nanosphere-masked PEDOT-OH

https://doi.org/10.1021/acsapm.3c01964
ACS Appl. Polym. Mater. 2023, 5, 10105−10115

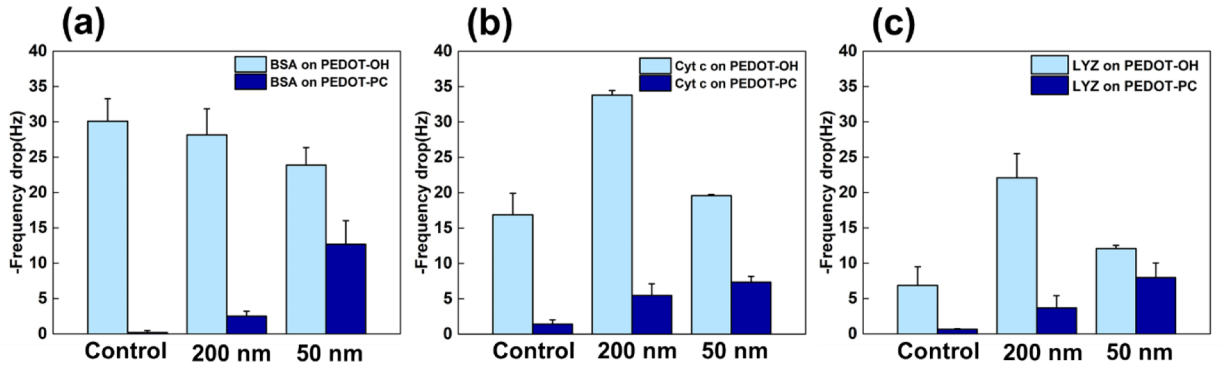

Figure 5. Statistical results of the frequency drop of three nonspecific binding proteins: (a) BSA, (b) LYZ, and (c) cyt *c*. The proteins were dissolved in PBS and analyzed under identical conditions (1 mg mL^{-1}) under a temperature control (25 °C).

sample (1 × 1 μm^2). In contrast to the adhesion pattern observed on the 200 nm nanosphere-masked PEDOT-OH template, no discernible periodic patterns were observed. Figure S7d,e displays the control experiment results, which included thin films of PEDOT-OH and PEDOT-PC without any patterns. Comparison of the adhesion properties of the two samples over a larger area (5 × 5 μm^2) demonstrated that the coating of PEDOT-PC led to a decrease in the overall adhesion. This reduction can be attributed to zwitterionic head groups, PC, that lower the surface tension between the AFM tip and the CP interface in the aqueous environment. Figure S7f illustrates the significant adhesion force observed on the 50 nm-masked PEDOT-OH sample (5 × 5 μm^2). Although well-defined patterns were not observed, periodic small pits on the surface resulted in an overall increase in adhesion.

The analysis of the AFM image depicted above highlights that the periodic concave-upward patterns significantly enhance the surface hydrogen bonding between the OH groups and the AFM tip. The curvature of these patterns effectively increases the total contact area of the probe with the OH groups, making it more challenging for the AFM tip to be pulled away from the patterned PEDOT-OH surface. These results underscore that the surface morphology substantially impacts the interface characteristics, as observed from a nanoscale perspective. Conversely, PC functional groups exhibit excellent lubricity in wet conditions and mitigate the surface structure's influence. PC lowers the overall surface tension due to its neutral net charge and strong affinity for water molecules.[51]

3.3. Nonspecific Protein Binding on the Patterned CP Interface. In evaluating nonspecific protein binding behavior on a patterned CP interface using QCM-D, we selected three proteins: BSA, LYZ, and cyt *c*. The frequency readout of QCM-D provided information about the total mass change on the substrate. When the flowing solution containing analytes made contact with the interface, the frequency decreased, indicating adsorption or binding events.

BSA, a globular protein commonly used as a blocking agent to prevent nonspecific binding on various sensing platforms, was employed in the study. BSA has a pI value of approximately 5, which results in a negative charge in PBS buffer (pH = 7.4). In contrast, PEDOTs typically exist in the oxidized state and carry a positive charge under various conditions. As a result, BSA is attracted to the interface due to electrostatic forces and forms a uniform coating between the protein solution and the CP. Adhesion mapping using AFM further illustrated that BSA diffusion at the interface led to a decrease in surface tension (Figure S8).

LYZ is a small lytic enzyme with a high pI value of about 11, whereas cyt *c* is a small hemeprotein consisting of 104 amino acids. The pI value of cyt *c* is lower than that of LYZ, which ranges from 9.0 to 10.65 depending on the analytical methods. Both LYZ and cyt *c* carry positive charges in the PBS buffer. The statistical result of the adsorption amount of three proteins was taken from the readout of the third overtone (n = 3) and summarized in Figure 5. Figure 5a shows that BSA exhibited a more substantial adsorption on the PEDOT-OH thin film, primarily due to the electrostatic attractive forces, compared to that of LYZ and cyt *c*. The adsorption mass on the 200 and 50 nm nanosphere-masked platforms showed a slight decrease compared to the control PEDOT-OH thin film. Previous studies have demonstrated that BSA molecules adsorbed to hydrophobic and hydrophilic surfaces with an α helical structure but had more affinity to hydrophilic surfaces after 12 h incubation.[52] Consequently, the amount of adsorbed BSA showed no distinct preference between the patterned PEDOT-OH and the unpatterned PEDOT thin film, in contrast to LYZ and cyt *c*. BSA is frequently used as a blocking agent to prevent further nonspecific binding by occupying the sides with high surface energy. The adhesion mapping on the 200 nm nanosphere-masked surfaces after BSA binding revealed a decrease in the total distribution of adhesion force (Figure S9b,e). The lowest value was set as the starting point of the colored scale bar in the AFM image. The color difference was significantly reduced after BSA blocking (from 2.5 nN for the 200 nm nanosphere-masked PEDOT-OH to 500 pN after BSA blocking). This result indicates that BSA effectively covers the CP film with or without nanopatterns, and the proteins fill in the cavities, decreasing overall surface adhesion.

Compared to the QCM-D results and WCA, the LYZ and cyt *c* binding trends differ from BSA results. LYZ, with the highest pI value, exhibited the lowest ΔF. For positively charged proteins such as LYZ and cyt *c*, fluid flow counteracted the affinity of the proteins to the positively charged PEDOT films, resulting in reduced protein binding to the surface. Interestingly, increased binding of cyt *c* and LYZ onto the 200 nm PS nanosphere-masked PEDOT-OH surface was observed through the QCM-D readout. Drawing from the previous work by Penna et al., molecular simulation studies on peptide adsorption can be divided into three steps. First, peptides diffuse from the bulk phase to the interface and locate biased sites. Second, the peptide anchors itself to the water−solid

https://doi.org/10.1021/acsapm.3c01964
ACS Appl. Polym. Mater. 2023, 5, 10105−10115

interface via hydrogen bonding between one of its hydrophilic groups and the water molecules adjacent to the surface. The final step involves the peptide firmly locking onto the surface through slow, stepwise, and largely sequential adsorption of its residues.[53] The AFM analysis mentioned earlier revealed that the 200 nm PS nanosphere-masked pattern on the PEDOT-OH platform induced stronger adhesion due to the hydrogen bonding of OH groups. Cavities also hindered the weak adsorption of positively charged proteins, preventing them from being rinsed away. These findings likely contributed to the significant increase in the frequency drop observed. Consequently, protein binding decreased on the 50 nm PS nanosphere-masked PEDOT-OH film due to an overall reduction in adhesion compared to the 200 nm platform (Figures S6b and S9b).

In contrast, a similar trend was observed for the three proteins on the PEDOT-PC template, which correlated with the WCA measurements. The relatively smooth CP film (control) exhibited a better antifouling ability. However, after the nanopatterns were created, the antifouling ability decreased. The surface roughness did not enhance the wettability of a hydrophilic material on the nanoscale even within a well-defined structure. The periodic nanopattern appeared to increase the energy barrier for the continuous water layer retained by PC groups, thus compromising their antifouling ability.[54] As a result, the total amount of nonspecific binding protein increased.

3.4. Specific Binding Protein CRP on the Patterned Interface. Human CRP is a nonspecific acute-phase plasma pentraxin that is produced by the liver. Typically, there are low concentrations of this protein in the blood. However, abnormal elevation of CRP is an indicator of underlying inflammation. Although the PC head groups can efficiently suppress the binding of other biomolecules, they are also suggested binding ligands for CRP recognition with membrane phospholipids in the presence of Ca^{2+}.[55] In this study, we also investigated the specific protein binding behavior involving CRP and Ca^{2+} ions in a HEPES buffer solution on both patterned PEDOT-OH and PEDOT-PC (Figure 6). Real-time QCM-D readouts are provided in Figure S10. CRP exhibited strong adsorption on PEDOT-OH. The results indicated a nonspecific CRP binding process on PEDOT-OH characterized by decreasing frequencies due to the adsorbed mass, an increase in dissipation reflecting energy dissipation decay within the protein layer, and dissipation returning to the baseline during the buffer rinsing in the final 15 min (Figure S10a–c).

PC is a hydrophilic headgroup that can retain a water layer at the interface. With a coating layer of PEDOT-PC, CRP can occupy PC positions, which are the binding sites in the presence of Ca^{2+}. The adsorbed protein layer is soft and loose packing for nonspecific binding, and the viscoelastic protein layer delays the oscillation propagating through the original polymer coating. The decay of the lost energy presents a positive value of dissipation of QCM-D analysis. However, an unusual dissipation drop occurred when the CRP proteins were binding to the PEDOT-PC film (Figure S10d). ΔD was the most significant feature that distinguished the templates with or without PC groups (Figure S10a,d). In previous studies, the water captured by the vicinity of PC could be released when the CRP recognition and the dissipation dropped during the binding process.[32,56] This phenomenon may result from substituting water molecules with CRP proteins. The release of water molecules stiffened the polymer

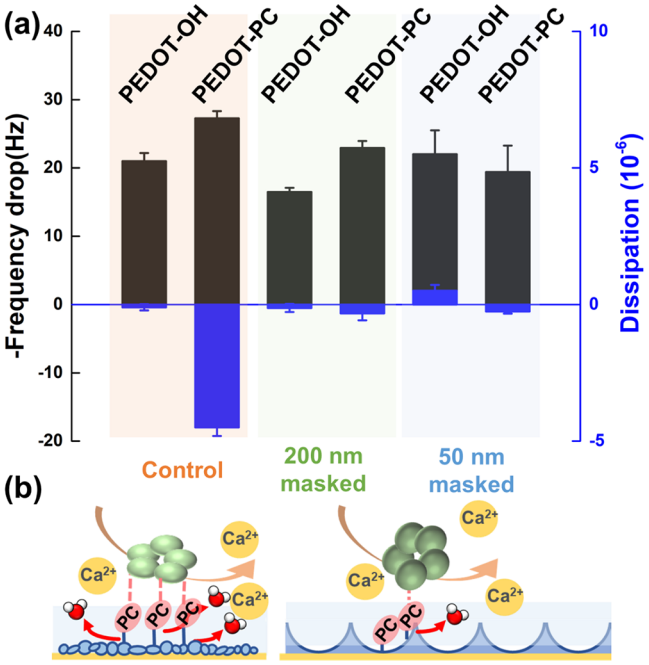

Figure 6. (a) Statistic of specific binding of CRP on different substrates. The black columns represent the frequency readout, and the blue columns represent the dissipation readout. (b) The schematic illustration of specific CRP binding on PEDOT-PC and patterned PEDOT-PC film.

film containing PC groups and evaluated the oscillation of the template that was sensed by QCM-D (a negative dissipation value).[57] When the nanopattern surface was created, the phenomenon of the dissipation drops simultaneously became unapparent (Figure S10e,f), although the total frequency drops seemed similar on each surface. From the previous kinetics study, the multivalent bindings of CRP can be enhanced under the optimal PC density.[16] From the QCM-D result, the nanostructured surface would also change the binding behavior of CRP on the PEDOT-PC film. The water release phenomenon disappeared as a result of the discontinuous water layer on the interface, which further corresponded to the WCA result illustrated with the Cassie–Baxter model. As a result, observing the specific binding of CRP could further explain why the patterned surface altered the interfacial water on the PEDOT-PC film.

4. CONCLUSIONS

In this study, a facile procedure to fabricate a CP platform was developed. The optimized conditions for manufacturing the nanotemplate via electrochemistry methods are provided. The PEDOT films are tunable with conducting CV in a three-electrode system. The scanning speed of the voltage and monomer concentration are the most critical variables for film thickness. The WCA of the nanostructure effect that competes with the surface hydrophilic functional groups better fits the Cassie–Baxter model on the concave-upward nanostructure. The air trapped inside the nanostructure may obstruct the water-wetting ability of the interface. We fully immersed the sample and conducted AFM in the liquid module to exclude the existence of a gas phase on the interface. The Peak Force QNM mode first revealed a periodic adhesive pattern on the nanostructured interface. The nanopatterned PEDOT-OH film presented a higher adhesive force in cavity regions due to the

https://doi.org/10.1021/acsapm.3c01964
ACS Appl. Polym. Mater. 2023, 5, 10105–10115

hydrogen bonding between OH groups with the silicon tip. This revealed that the nanostructure may alter the localized surface adhesion. On the other hand, the zwitterionic PC moiety significantly lowered the total surface tension, and the periodic pattern became invisible. The further force−volume mapping provided a more accurate measurement of the localized pull-out force on patterned interfaces with force−distance curves. Localizing counterions on phosphorylcholine groups captured a tight layer of water molecules, preventing nonspecific fouling. The AFM results also proved no sensing of the interaction force on the PC coating interface. The analysis on the nanoscale could provide more details of the zwitterionic effect of the air−water interface.

According to the QCM-D measurements, there were distinct patterns in nonspecific protein binding when positively and negatively charged proteins were considered. Negatively charged BSA easily binds to the PEDOT film because of the electrostatic attraction. However, the positively charged proteins show a higher binding mass on 200 nm PS nanosphere-masked PEDOT-OH due to the nanostructure's localized attraction of hydrogen bonding. The nonspecific binding on PEDOT-PC all followed the trends of WCA results. The specific binding of the CRP protein to PC was also involved in the study. When substituting the water molecules for CRP proteins on the PC-modified interface, the surface becomes more rigid, measured by QCM-D. However, creating the patterns on the interface with PEDOT-PC dramatically decreased the water release during the CRP binding, indicating the poor formation of the water layer on the nanostructured PEDOT-PC. The nanopattern not only restricts the specific CRP binding but also interrupts the water layer formation on the surface of PEDOT-PC. This study offers a more profound understanding of the adhesion force's surface characteristics concerning nanostructures on two distinct functional groups. Furthermore, it assesses how nanostructures influence antifouling properties, illuminating the interplay between nanostructured surfaces and proteins within biotechnological contexts.

■ ASSOCIATED CONTENT

Supporting Information

The Supporting Information is available free of charge at https://pubs.acs.org/doi/10.1021/acsapm.3c01964.

FTIR spectra, XPS survey spectrum, and cyclic voltammograms of polymers; AFM images showing topography and adhesion mapping; and real-time frequency and dissipation readouts of CRP binding by QCM-D (PDF)

■ AUTHOR INFORMATION

Corresponding Authors

Jie-Ren Li − *Department of Chemistry, National Cheng Kung University, Tainan 70101, Taiwan;* orcid.org/0000-0001-8336-0092; Email: jierenli@mail.ncku.edu.tw

Shyh-Chyang Luo − *Department of Materials Science and Engineering, National Taiwan University, Taipei 10617, Taiwan; Institute of Biomedical Engineering and Nanomedicine, National Health Research Institutes, Miaoli County 35053, Taiwan;* orcid.org/0000-0003-3972-1086; Email: shyhchyang@ntu.edu.tw

Authors

Chia-Hsin Lin − *Department of Materials Science and Engineering, National Taiwan University, Taipei 10617, Taiwan*

Chang-Yun Wang − *Department of Chemistry, National Cheng Kung University, Tainan 70101, Taiwan*

Complete contact information is available at: https://pubs.acs.org/10.1021/acsapm.3c01964

Notes

The authors declare no competing financial interest.

■ ACKNOWLEDGMENTS

We gratefully acknowledge the financial support provided by the National Science and Technology Council of Taiwan (NSTC 111-2113-M-002-020-MY3 and 112-2113-M-006-013).

■ ABBREVIATIONS

PEDOT, poly(3,4-ethylenedioxythiophene); PC, phosphorylcholine; OH, hydroxyl; PEDOT-OH, hydroxyl-functionalized; PEDOT-PC, phosphorylcholine-functionalized; FTIR, Fourier-transform infrared spectroscopy; CV, cyclic voltammogram; AFM, atomic force microscopy; BSA, bovine serum albumin; LYZ, lysozyme; CRP, C-reactive protein; cyt *c*, cytochrome *c*; MPC, 2-methacryloyloxyethyl phosphorylcholine; PS, polystyrene; CP, conducting polymer; PFQNM, Peak Force Quantitative Nanomechanical Mapping; QCM-D, quartz crystal microbalance with dissipation; WCA, water contact angle

■ REFERENCES

(1) Spori, D. M.; Drobek, T.; Zürcher, S.; Ochsner, M.; Sprecher, C.; Mühlebach, A.; Spencer, N. D. Beyond the Lotus Effect: Roughness Influences on Wetting over a Wide Surface-Energy Range. *Langmuir* **2008**, *24* (10), 5411−5417.

(2) Yamamoto, M.; Nishikawa, N.; Mayama, H.; Nonomura, Y.; Yokojima, S.; Nakamura, S.; Uchida, K. Theoretical Explanation of the Lotus Effect: Superhydrophobic Property Changes by Removal of Nanostructures from the Surface of a Lotus Leaf. *Langmuir* **2015**, *31* (26), 7355−7363.

(3) Yu, L.; Tang, P.; Nie, C.; Hou, Y.; Haag, R. Well-Defined Nanostructured Biointerfaces: Strengthened Cellular Interaction for Circulating Tumor Cells Isolation. *Adv. Healthcare Mater.* **2021**, *10* (11), No. e2002202.

(4) Ma, Y.; Tian, X.; Liu, L.; Pan, J.; Pan, G. Dynamic Synthetic Biointerfaces: From Reversible Chemical Interactions to Tunable Biological Effects. *Acc. Chem. Res.* **2019**, *52* (6), 1611−1622.

(5) Chang, B.; Zhang, M.; Qing, G.; Sun, T. Dynamic biointerfaces: from recognition to function. *Small* **2015**, *11* (9−10), 1097−1112.

(6) Velev, O. D.; Kaler, E. W. In Situ Assembly of Colloidal Particles into Miniaturized Biosensors. *Langmuir* **1999**, *15* (11), 3693−3698.

(7) Jiang, P. Wafer-scale fabrication of periodic polymer attolitre microvial arrays. *Chem. Commun.* **2005**, *13*, 1699−1701.

(8) Fustin, C.-A.; Glasser, G.; Spiess, H. W.; Jonas, U. Parameters Influencing the Templated Growth of Colloidal Crystals on Chemically Patterned Surfaces. *Langmuir* **2004**, *20* (21), 9114−9123.

(9) Park, J. Y.; Pernites, R.; Estillore, N.; Hyakutake, T.; Ponnapati, R.; Tiu, B. D.; Nishide, H.; Advincula, R. C. Capsulation of carbon nanotubes on top of colloidally templated and electropolymerized polythiophene arrays. *Chem. Commun.* **2011**, *47* (31), 8871−8873.

(10) Pernites, R. B.; Felipe, M. J.; Foster, E. L.; Advincula, R. C. Colloidally templated two-dimensional conducting polymer arrays and SAMs: binary composition patterning and chemistry. *ACS Appl. Mater. Interfaces* **2011**, *3* (3), 817−827.

(11) Lin, W. F.; Swartz, L. A.; Li, J. R.; Liu, Y.; Liu, G. Y. Particle Lithography Enables Fabrication of Multicomponent Nanostructures. *J. Phys. Chem. C* **2013**, *117* (44), 23279−23285.
(12) Guang, J.; Lu, M.; Liu, Y.; Fan, R.; Wang, C.; Li, R.; Liang, Y.; Peng, W. Flexible and Speedy Preparation of Large-Scale Polystyrene Monolayer through Hemispherical-Depression-Assisted Self-Assembling and Vertical Lifting. *ACS Appl. Polym. Mater.* **2023**, *5* (4), 2674−2683.
(13) Walker, E. J.; Pandiyarajan, C. K.; Efimenko, K.; Genzer, J. Generating Surface-Anchored Zwitterionic Networks and Studying Their Resistance to Bovine Serum Albumin Adsorption. *ACS Appl. Polym. Mater.* **2019**, *1* (12), 3323−3333.
(14) Lau, S. K.; Yong, W. F. Recent Progress of Zwitterionic Materials as Antifouling Membranes for Ultrafiltration, Nanofiltration, and Reverse Osmosis. *ACS Appl. Polym. Mater.* **2021**, *3* (9), 4390−4412.
(15) Higaki, Y.; Nishida, J.; Takenaka, A.; Yoshimatsu, R.; Kobayashi, M.; Takahara, A. Versatile inhibition of marine organism settlement by zwitterionic polymer brushes. *Polym. J.* **2015**, *47* (12), 811−818.
(16) Goda, T.; Ishihara, K.; Miyahara, Y. Critical update on 2-methacryloyloxyethyl phosphorylcholine (MPC) polymer science. *J. Appl. Polym. Sci.* **2015**, *132* (16), n/a-n/a.
(17) Azuma, T.; Ohmori, R.; Teramura, Y.; Ishizaki, T.; Takai, M. Nano-structural comparison of 2-methacryloyloxyethyl phosphorylcholine- and ethylene glycol-based surface modification for preventing protein and cell adhesion. *Colloids Surf., B* **2017**, *159*, 655−661.
(18) Brown, M. U.; Triozzi, A.; Emrick, T. Polymer Zwitterions with Phosphonium Cations. *J. Am. Chem. Soc.* **2021**, *143* (17), 6528−6532.
(19) Zhu, B.; Luo, S. C.; Zhao, H.; Lin, H. A.; Sekine, J.; Nakao, A.; Chen, C.; Yamashita, Y.; Yu, H. H. Large enhancement in neurite outgrowth on a cell membrane-mimicking conducting polymer. *Nat. Commun.* **2014**, *5*, 4523.
(20) Pan, Q.; Wu, Q.; Sun, Q.; Zhou, X.; Cheng, L.; Zhang, S.; Yuan, Y.; Zhang, Z.; Ma, J.; Zhang, Y.; Zhu, B. Biomolecule-friendly conducting PEDOT interface for long-term bioelectronic devices. *Sens. Actuators, B* **2022**, *373*, No. 132703.
(21) Luo, S.-C.; Mohamed Ali, E.; Tansil, N. C.; Yu, H.-h.; Gao, S.; Kantchev, E. A. B.; Ying, J. Y. Poly(3,4-ethylenedioxythiophene) (PEDOT) Nanobiointerfaces: Thin, Ultrasmooth, and Functionalized PEDOT Films with in Vitro and in Vivo Biocompatibility. *Langmuir* **2008**, *24* (15), 8071−8077.
(22) Zhang, Y. Q.; Lin, H. A.; Pan, Q. C.; Qian, S. H.; Zhang, S. H.; Qiu, G.; Luo, S. C.; Yu, H. H.; Zhu, B. Tunable Protein/Cell Binding and Interaction with Neurite Outgrowth of Low-Impedance Zwitterionic PEDOTs. *ACS Appl. Mater. Interfaces* **2020**, *12* (10), 12362−12372.
(23) Zhu, Y.; Lin, H.-A.; Zhang, S.; Pan, Q.; Qian, S.; Zhang, S.; Zhang, Y.; Luo, S.-C.; Yu, H.-H.; Zhu, B. A straightforward strategy to spatially organize repulsive and attractive cues on Zwitterionic PEDOTs. *Colloid Interface Sci. Commun.* **2022**, *50*, No. 100656.
(24) Uhlig, M. R.; Garcia, R. In Situ Atomic-Scale Imaging of Interfacial Water under 3D Nanoscale Confinement. *Nano Lett.* **2021**, *21* (13), 5593−5598.
(25) Fukuma, T.; Garcia, R. Atomic- and Molecular-Resolution Mapping of Solid-Liquid Interfaces by 3D Atomic Force Microscopy. *ACS Nano* **2018**, *12* (12), 11785−11797.
(26) Oras, S.; Vlassov, S.; Berholts, M.; Lohmus, R.; Mougin, K. Tuning adhesion forces between functionalized gold colloidal nanoparticles and silicon AFM tips: role of ligands and capillary forces. *Beilstein J. Nanotechnol.* **2018**, *9*, 660−670.
(27) Dupont-Gillain, C. C.; Jacquemart, I. Patterned collagen layers on polystyrene: direct probing using AFM in the adhesion mapping mode. *Surf. Sci.* **2003**, *539* (1), 145−154.
(28) Garcia, R. Nanomechanical mapping of soft materials with the atomic force microscope: methods, theory and applications. *Chem. Soc. Rev.* **2020**, *49*, 5850.
(29) Easley, A. D.; Ma, T.; Eneh, C. I.; Yun, J.; Thakur, R. M.; Lutkenhaus, J. L. A practical guide to quartz crystal microbalance with dissipation monitoring of thin polymer films. *J. Polym. Sci.* **2022**, *60* (7), 1090−1107.
(30) Tagaya, M. In situ QCM-D study of nano-bio interfaces with enhanced biocompatibility. *Polym. J.* **2015**, *47* (9), 599−608.
(31) Dudchenko, A. V.; Bengani-Lutz, P.; Asatekin, A.; Mauter, M. S. Foulant Adsorption to Heterogeneous Surfaces with Zwitterionic Nanoscale Domains. *ACS Appl. Polym. Mater.* **2020**, *2* (11), 4709−4718.
(32) Wu, J. G.; Wei, S. C.; Chen, Y.; Chen, J. H.; Luo, S. C. Critical Study of the Recognition between C-Reactive Protein and Surface-Immobilized Phosphorylcholine by Quartz Crystal Microbalance with Dissipation. *Langmuir* **2018**, *34* (3), 943−951.
(33) Chin, M.; Tada, S.; Tsai, M. H.; Ito, Y.; Luo, S. C. Strategy to Immobilize Peptide Probe Selected through In Vitro Ribosome Display for Electrochemical Aptasensor Application. *Anal. Chem.* **2020**, *92* (16), 11260−11267.
(34) Ozeki, T.; Morita, M.; Yoshimine, H.; Furusawa, H.; Okahata, Y. Hydration and Energy Dissipation Measurements of Biomolecules on a Piezoelectric Quartz Oscillator by Admittance Analyses. *Anal. Chem.* **2007**, *79* (1), 79−88.
(35) Kumar, S.; Ye, F.; Dobretsov, S.; Dutta, J. Nanocoating Is a New Way for Biofouling Prevention. *Front. Nanotechnol.* **2021**, *3*, No. 771098, DOI: 10.3389/fnano.2021.771098.
(36) Jiang, X.; Shao, Y.; Li, J.; Wu, M.; Niu, Y.; Ruan, X.; Yan, X.; Li, X.; He, G. Bioinspired Hybrid Micro/Nanostructure Composited Membrane with Intensified Mass Transfer and Antifouling for High Saline Water Membrane Distillation. *ACS Nano* **2020**, *14* (12), 17376−17386.
(37) He, M.; Gao, K.; Zhou, L.; Jiao, Z.; Wu, M.; Cao, J.; You, X.; Cai, Z.; Su, Y.; Jiang, Z. Zwitterionic materials for antifouling membrane surface construction. *Acta Biomater.* **2016**, *40*, 142−152.
(38) Andersson, J.; Jarlebark, J.; Kk, S.; Schaefer, A.; Hailes, R.; Palasingh, C.; Santoso, B.; Vu, V. T.; Huang, C. J.; Westerlund, F.; Dahlin, A. Polymer Brushes on Silica Nanostructures Prepared by Aminopropylsilatrane Click Chemistry: Superior Antifouling and Biofunctionality. *ACS Appl. Mater. Interfaces* **2023**, *15* (7), 10228−10239.
(39) Rybczynski, J.; Ebels, U.; Giersig, M. Large-scale, 2D arrays of magnetic nanoparticles. *Colloids Surf., A* **2003**, *219* (1−3), 1−6.
(40) Van Gorp, H.; Walke, P.; Braganca, A. M.; Greenwood, J.; Ivasenko, O.; Hirsch, B. E.; De Feyter, S. Self-Assembled Polystyrene Beads for Templated Covalent Functionalization of Graphitic Substrates Using Diazonium Chemistry. *ACS Appl. Mater. Interfaces* **2018**, *10* (14), 12005−12012.
(41) Chow, T. S. Wetting of rough surfaces. *J. Phys.: Condens.* **1998**, *10* (27), L445.
(42) Abdelsalam, M. E.; Bartlett, P. N.; Kelf, T.; Baumberg, J. Wetting of Regularly Structured Gold Surfaces. *Langmuir* **2005**, *21* (5), 1753−1757.
(43) Koch, B. M. L.; Amirfazli, A.; Elliott, J. A. W. Wetting of Rough Surfaces by a Low Surface Tension Liquid. *J. Phys. Chem. C* **2014**, *118* (41), 23777−23782.
(44) Shardt, N.; Elliott, J. A. W. Gibbsian Thermodynamics of Cassie−Baxter Wetting (Were Cassie and Baxter Wrong? Revisited). *Langmuir* **2018**, *34* (40), 12191−12198.
(45) Olubowale, O. H.; Biswas, S.; Azom, G.; Prather, B. L.; Owoso, S. D.; Rinee, K. C.; Marroquin, K.; Gates, K. A.; Chambers, M. B.; Xu, A.; Garno, J. C. "May the Force Be with You!" Force-Volume Mapping with Atomic Force Microscopy. *ACS Omega* **2021**, *6* (40), 25860−25875.
(46) Medalsy, I.; Hensen, U.; Muller, D. J. Imaging and quantifying chemical and physical properties of native proteins at molecular resolution by force-volume AFM. *Angew. Chem., Int. Ed.* **2011**, *50* (50), 12103−12108.
(47) Attard, P.; Miklavcic, S. J. Effective Spring Constant of Bubbles and Droplets. *Langmuir* **2001**, *17* (26), 8217−8223.
(48) Zhang, X. H.; Maeda, N.; Craig, V. S. J. Physical Properties of Nanobubbles on Hydrophobic Surfaces in Water and Aqueous Solutions. *Langmuir* **2006**, *22* (11), 5025−5035.

(49) An, H.; Liu, G.; Atkin, R.; Craig, V. S. J. Surface Nanobubbles in Nonaqueous Media: Looking for Nanobubbles in DMSO, Formamide, Propylene Carbonate, Ethylammonium Nitrate, and Propylammonium Nitrate. *ACS Nano* **2015**, *9* (7), 7596−7607.
(50) An, H.; Tan, B. H.; Ohl, C. D. Distinguishing Nanobubbles from Nanodroplets with AFM: The Influence of Vertical and Lateral Imaging Forces. *Langmuir* **2016**, *32* (48), 12710−12715.
(51) Higaki, Y.; Furusawa, R.; Otsu, T.; Yamada, N. L. Zwitterionic Poly(carboxybetaine) Brush/Albumin Conjugate Films: Structure and Lubricity. *Langmuir* **2022**, *38* (30), 9278−9284.
(52) Jeyachandran, Y. L.; Mielczarski, E.; Rai, B.; Mielczarski, J. A. Quantitative and Qualitative Evaluation of Adsorption/Desorption of Bovine Serum Albumin on Hydrophilic and Hydrophobic Surfaces. *Langmuir* **2009**, *25* (19), 11614−11620.
(53) Penna, M. J.; Mijajlovic, M.; Biggs, M. J. Molecular-level understanding of protein adsorption at the interface between water and a strongly interacting uncharged solid surface. *J. Am. Chem. Soc.* **2014**, *136* (14), 5323−5331.
(54) Murakami, D.; Jinnai, H.; Takahara, A. Wetting transition from the Cassie-Baxter state to the Wenzel state on textured polymer surfaces. *Langmuir* **2014**, *30* (8), 2061−2067.
(55) Park, J.; Kurosawa, S.; Watanabe, J.; Ishihara, K. Evaluation of 2-Methacryloyloxyethyl Phosphorylcholine Polymeric Nanoparticle for Immunoassay of C-Reactive Protein Detection. *Anal. Chem.* **2004**, *76* (9), 2649−2655.
(56) Wu, J. G.; Wei, S. C.; Luo, S. C. In Situ Probing Unusual Protein Adsorption Behavior on Electrified Zwitterionic Conducting Polymers. *Adv. Mater. Interfaces* **2020**, *7* (15), No. 2000470, DOI: 10.1002/admi.202000470.
(57) Goda, T.; Miyahara, Y. Engineered zwitterionic phosphorylcholine monolayers for elucidating multivalent binding kinetics of C-reactive protein. *Acta Biomater* **2016**, *40*, 46−53.